sustainability

MDPI

Article

Sustainable Recovery of CO_2 by Using Visible-Light-Responsive Crystal Cuprous Oxide/Reduced Graphene Oxide

Shou-Heng Liu [1,*], Jun-Sheng Lu [1] and Yi-Chiun Chen [1,2]

1 Department of Environmental Engineering, National Cheng Kung University, Tainan 70101, Taiwan; dalelu4404@gmail.com (J.-S.L.); z10308032@email.ncku.edu.tw (Y.-C.C.)
2 Department of Resources Engineering, National Cheng Kung University, Tainan 701, Taiwan
* Correspondence: shliu@mail.ncku.edu.tw; Tel.: +886-6-2757575 (ext. 65843)

Received: 5 September 2018; Accepted: 31 October 2018; Published: 11 November 2018

Abstract: A simple solution-chemistry method has been investigated to prepare crystal cuprous oxide (Cu_2O) incorporated with reduced graphene oxide (designated as Cu_2O-rGO-x, where x represents the contents of rGO = 1%, 5% and 10%) in this work. These Cu_2O-rGO-x composites combine the prospective advantages of rhombic dodecahedra Cu_2O together with rGO nanosheets which have been studied as visible-light-sensitive catalysts for the photocatalytic production of methanol from CO_2. Among the Cu_2O-rGO-x photocatalysts, the methanol yield photocatalyzed by Cu_2O-rGO-5% can be observed to be 355.26 μmol g^{-1}cat, which is ca. 36 times higher than that of pristine Cu_2O nanocrystal in the 20th hour under visible light irradiation. The improved activity may be attributed to the enhanced absorption ability of visible light, the superior separation of electron–hole pairs, well-dispersed Cu_2O nanocrystals and the increased photostability of Cu_2O, which are evidenced by employing UV-vis diffuse reflection spectroscopy, photoluminescence, scanning electron microscopy/transmission electron microscopy and X-ray photoelectron spectroscopy, respectively. This work demonstrates an easy and cost-effective route to prepare non-noble photocatalysts for efficient CO_2 recovery in artificial photosynthesis.

Keywords: cuprous oxide; solar energy; graphene; visible-light-driven; CO_2 conversion

1. Introduction

In the past decades, global warming, which is causing serious global climate change problems and ocean acidification, has been becoming more and more severe with the increase of greenhouse gases (e.g., carbon dioxide) [1]. A global agreement to reduce greenhouse gases has been reached on the COP21 in Paris on December 2015. In order to reduce CO_2 emissions, technologies developed for carbon capture, storage and utilization (CCSU) have been widely implemented [2,3]. Among these possible technologies, the conversion of CO_2 into useful chemicals or fuels is considered as one of the most promising approaches to deal with energy and environmental issues at the same time [4–6]. However, extra energy is required for the transformation of CO_2 because it is a stable molecule ($\Delta G = -400$ kJ mol^{-1}) value [7]. Therefore, CO_2 conversion via photocatalytic reactions, which are involved in the utilization of solar energy, is an eco-friendly attractive route [8–12]. Previous studies [13–16] revealed that photocatalysts consisting of metal oxides are shown to be active in the UV-light region. However, it is difficult to practically use the aforementioned photocatalysts due to the limited fraction of the UV spectrum in natural sunlight [17–19]. Therefore, developments in visible-light-driven photocatalysts for artificial photosynthesis are crucial. To address this issue, many works have focused on enhancing the visible-light-active photocatalysts by using methods

such as doping the semiconductors with non-metal/metal ions [20–23], engineering semiconductor structures [24], exposing a facet of the semiconductors [21,25–27], and semiconductor coupling [28,29]. As a result, these prepared photocatalysts, by using the above-mentioned routes, possess better charge carrier transfer, hence leading to a notable improvement in the photocatalytic performance under visible light.

Cuprous oxides (Cu_2O), which are p-type semiconductors, have been widely investigated for visible-light-responsive photocatalysis in artificial photosynthesis owing to their low cost, small band gap (ca. 2.0–2.2 eV) and suitable energy level of conduction and valence bands [15,30–32]. It is extensively reported that the Cu_2O nanocrystals can highly enhance the photocatalytic oxidation of organic pollutants under visible-light irradiation [33–37]. However, the studies on the photocatalytic reduction of CO_2 via crystal Cu_2O are limited. In the earlier report [38], the different facets of Cu_2O were investigated to perform the photocatalytic reduction of CO_2, indicating that the low-index facets of Cu_2O possessed higher activity than Cu_2O with higher index facets. In addition, Cu_2O with a stone-like shape exhibited superior activity to that with nanobelt arrays in terms of CO_2 photoreduction [39]. Nevertheless, the crystal Cu_2O applied in the photocatalytic reactions suffers from the separation of photogenerated electron–hole pairs [31] and long-term stability [40]. Recently, the enhanced durability and activity [41–46] can be achieved by the Cu_2O-based photocatalysts. Among them, the incorporation of graphene with the 2D sp^2-hybridized carbons has received much attention due to its high electron mobility [47], theoretical surface area [48], and chemical stability [49]. For instance, a microwave-assisted chemical method was proposed to prepare Cu_2O/reduced graphene oxide (rGO) nanocomposites which have improved activity and stability toward the photocatalytic reduction of CO_2 [50]. Spherical Cu_2O nanoparticles were incorporated with rGO by using in-situ reduction method, and their photocatalytic activities toward CO_2 reduction were better than that of pristine Cu_2O nanoparticles [51]. Although the synthesis of Cu_2O–graphene composites with visible-light-active CO_2 reduction was proposed previously, the crystal structure of Cu_2O decorated with rGO in the photoreduction of CO_2 was reported for the first time.

In the present research, the nanocrystal Cu_2O-possessing facets decorated with various amounts of rGO nanosheets (named as Cu_2O-rGO-x, x = amounts of rGO) were synthesized by using a simple solution-chemical method. The resultant Cu_2O-rGO-x photocatalysts were thoroughly characterized via a variety of spectroscopic analyses. Also, the tests regarding the photoreduction of CO_2 under visible light show that rhombic dodecahedral Cu_2O decorated with 5 wt.% of rGO exhibited superior photocatalytic activity to the other Cu_2O-rGO-x and pristine Cu_2O. The reaction mechanism in the enhancement of CO_2 photoreduction by Cu_2O-rGO-5% composites is studied and discussed later.

2. Materials and Methods

2.1. Preparation of Crystal Cu_2O Decorated with rGO

Graphene oxide (GO) was fabricated by using the modified Hummer's method based on the earlier work [52]. For the synthesis of crystal Cu_2O decorated with rGO, fixed amounts of 0.1 M $CuCl_2$ and sodium dodecyl sulfate (SDS, Sigma, St. Louis, MO, USA, 99%) were added into various weight ratios of GO solution (1–10%) under stirring in a water bath at 34 °C. After 20 min, 1.8 mL of 1 M NaOH solution was added into the mixed solution, and then it was stirred for 20 s. Twenty-four milliliters of 0.1 M $NH_2OH{\cdot}HCl$ (Alfa Aesar, Haverhill, MA, USA, 99%) solution was slowly poured into the mixture. The mixture was stirred for 20 s and kept in the water bath for an hour. Finally, the product was washed and then separated by a centrifuge several times. After that, these precipitates were dried in vacuum at 30 °C for 8 h. The resultant products were symbolized as Cu_2O-rGO-x (x represents the amounts of rGO = 1%, 5% and 10%).

2.2. Characterizations

X-ray diffraction (XRD) measurements were carried out by a PANalytical X'Pert PRO diffractometer (Cu Kα, λ = 1.541 Å) at a scan of 3° min^{-1} from 5 to 80°. The morphologies of samples were identified by scanning electron microscopy (SEM) and transmission electron microscopy on a field-emission scanning electron microscope (JSM-7000F, JEOL, Akishima, Tokyo, Japan) and transmission electron microscope (JEM-1400, JEOL, Akishima, Tokyo, Japan) with respective accelerating voltages of 20 and 200 kV. The rate of the electron–hole recombination of photocatalysts can be determined by photo-luminescence (HR800, HORIBA, Kyoto, Japan) from 450 to 650 nm. X-ray photoelectron spectra (XPS) were recorded via a Kratos AXIS Ultra DLD spectrometer system with an excitation source of Al Kα (1486 eV). The peak of adventitious carbon (284.6 eV) was referenced to calibrate the binding energies of the photoelectrons. The electrons could be excited from the valance band to the conduction band of the sample by excitation light with 325 nm. The spectra of diffuse reflectance ultraviolet/visible (UV/Vis) light were taken on a spectrophotometer (Cary 100, Varian, Palo Alto, CA, USA).

2.3. Photoreduction of CO_2 Experiments

The photocatalytic activity measurements were carried out in a batch reactor (200 mL) equipped with a water-circulation cooling system. About 25 mg of samples and 50 mL of deionized water (DI) water were added into the aforementioned reactor, followed by dispersing homogeneously in water by sonication. Then, pure CO_2 gas (99.995%) was introduced into the reactor for 45 min to keep the solution saturated and ensure adsorption–desorption equilibrium in the dark. After the reactor was sealed, the photocatalytic reaction was performed by using a top-irradiated 300W Xe lamp (Model 66142, Newport, Irvine, CA, USA) with a cut-off filter to remove UV illumination. During the reaction process, the gas (1 mL) and liquid (1 μL) products were withdrawn periodically and examined by gas chromatography (GC, GC-430, Bruker, Billerica, MA, USA) with a thermal conductivity detector (TCD, equipped with molecular sieve 5A column) and a barrier discharge ionization detector (BID, GC-2010 Plus equipped with DB-WAXETR column, Shimadzu, Kyoto, Japan), respectively.

3. Results and Discussion

The X-ray diffraction patterns of GO, crystal Cu_2O and Cu_2O-rGO-*x* composites (*x* represents the weight percentage of rGO to Cu_2O) are shown in Figure 1. The results show that all the diffraction features of crystal Cu_2O-rGO-*x* composites are located at 2θ of 29.6°, 36.4°, 42.3°, 61.4°, 73.6° and 77.5° which can be assigned to (110), (111), (200), (220), (311), and (222), respectively. This indicates the presence of a crystal phase of Cu_2O (JCPDS #78-2076) in the Cu_2O-rGO-*x* composites. No characteristic peak of GO at 2θ = 10.6° can be observed for all samples, suggesting that the GO may be reduced to rGO. No characteristic peaks of rGO can be found for all Cu_2O-rGO-*x* samples in the X-ray diffraction patterns, which may be due to the lower contents of rGO and higher intensity of crystal Cu_2O. As reported previously [53], the crystal structure of Cu_2O is a pure rhombic dodecahedron when the intensity ratio of the (220) facet to the (200) facet (I_{220}/I_{200}) is 0.79. The values of I_{220}/I_{200} of Cu_2O and Cu_2O-rGO-*x* (*x* = 1%, 5% and 10%) are calculated to be 0.76, 0.72, 0.58, and 0.56, respectively. It can be found that the values of I_{220}/I_{200} are decreased when the contents of rGO in the Cu_2O-rGO-*x* composites are increased. The I_{220}/I_{200} of Cu_2O-rGO-10% is decreased to 0.56 while the weight ratio of rGO is increased to 10%. There are two possible reasons which could explain why the crystal structure of rhombic dodecahedral Cu_2O cannot be completely formed. First, the pH of the solution was changed from neutral to acidic by adding GO, which may hinder the formation of a crystal structure of Cu_2O. Second, GO would react with the reductant to form rGO during the synthesis process. This would lead to insufficient amounts of the reductant for the formation of a crystal structure of rhombic dodecahedral Cu_2O [53].

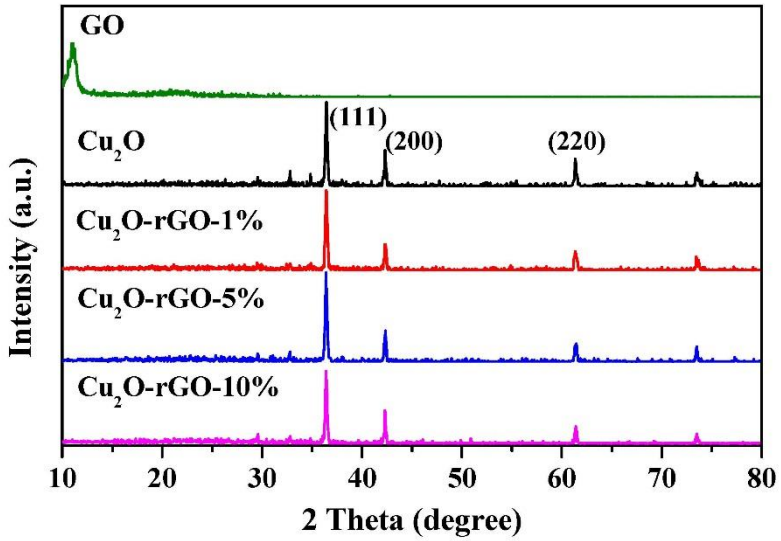

Figure 1. Powdered XRD patterns of graphene oxide (GO), Cu_2O and various Cu_2O-rGO-*x* photocatalysts.

The high-resolution scanning electron microscope (SEM) was used to investigate the morphology of Cu_2O-rGO-*x* composites. The SEM clearly presents the morphology of rGO with numerous wrinkles on the surface, as shown in Figure 2. In addition, the rhombic dodecahedral structure of Cu_2O nanocrystals can be observed. The SEM images of Cu_2O-rGO-1% demonstrates that the morphologies of Cu_2O nanocrystals remain as rhombic dodecahedra and the rGO sheet was successfully incorporated onto Cu_2O nanocrystals. However, the aggregation of Cu_2O nanocrystals in the Cu_2O-rGO-1% composites can be observed since the amounts of rGO in the composites is limited. Upon incorporating higher amounts of rGO into the composites, the Cu_2O crystals in the Cu_2O-rGO-5% and Cu_2O-rGO-10% are found to have a better dispersion on rGO sheets. Nevertheless, the destruction of rhombic dodecahedral Cu_2O nanocrystals can be observed for Cu_2O-rGO-*x* (x = 5% and 10%). In particular, the crystallization structure of Cu_2O-rGO-10% composites could hardly be seen, as shown in Figure 2. This is in good accordance with the aforementioned XRD results.

The transmission electron microscopy (TEM) image of rGO shows a thin sheet with wrinkles, similar to paper, as displayed in Figure 2. The deeper-colored region can be observed in the TEM image of rGO, which may be caused by the stack of rGO sheets. The wrinkles on the rGO sheets could result in a higher surface area of rGO, which may enhance the capacity of CO_2 adsorption. Therefore, it is helpful that rGO was decorated onto the surface of Cu_2O nanocrystals. The morphological and structural features of Cu_2O and Cu_2O-rGO-*x* composites (x = 1%, 5% and 10%) were also studied by TEM and their corresponding images are shown in Figure 2. It can be seen that the morphological features of rhombic dodecahedral Cu_2O are similar to a honey-comb shape with a particle size of 400–500 nm. As can be seen from the inset of Figure 2, the corresponding selected-area electron diffraction (SAED) pattern of rhombic dodecahedra can be observed along the [100] direction. The TEM images also show that Cu_2O nanocrystals are decorated with thin rGO sheets with some wrinkles. This result confirms that rGO is successfully decorated on rhombic dodecahedral Cu_2O.

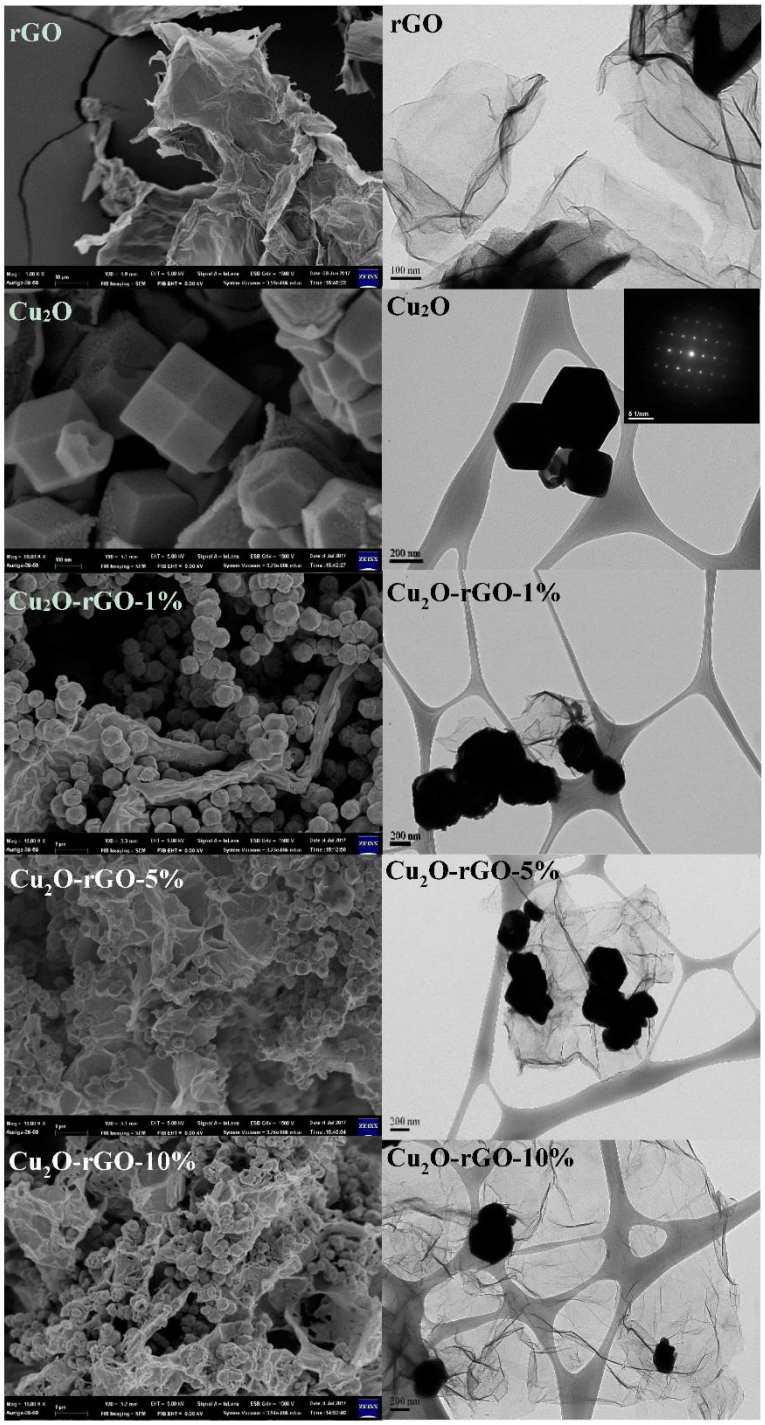

Figure 2. SEM and TEM images of rGO, Cu_2O and Cu_2O-rGO-x (x = 1%, 5% and 10%).

The elemental compositions and the chemical surface states of GO, rGO, crystal Cu_2O and Cu_2O-rGO-x composites were examined by XPS. In Figure 3a, the survey scans of the samples suggest the existence of carbon, oxygen and copper. The high-resolution C1s XPS spectra of GO (see Figure 3b) indicate three deconvoluted peaks at 284.6, 286.7, and 289.1 eV, which are ascribed to C–C/C=C, C–O, and C=O/COOH bonds, respectively. The intensities of C–O bindings found for rGO and Cu_2O-rGO-x samples are decreased, indicating that GO can be effectively reduced to rGO in the Cu_2O-rGO-x. As can be seen from Figure 3c, the Cu2p XPS spectra of Cu_2O-rGO-x composites display two major peaks at ca. 932.6 and 952.4 eV corresponding to Cu(I) $2p_{3/2}$ and Cu(I) $2p_{1/2}$,

respectively. Moreover, the binding energies of 934.8 and 954.3 eV are attributed to the formation of Cu(II), indicating the presence of Cu(II) on the surface of Cu_2O and Cu_2O-rGO-*x* photocatalysts. However, the intensities of aforementioned peaks (i.e., Cu(II)) are obviously reduced for Cu_2O-rGO-5% and Cu_2O-rGO-10% composites, implying the prevention of surface oxidation of Cu_2O. It can be attributed to the enhancement of chemical stability caused by improving the electronic structure of Cu_2O nanocrystals in the presence of carbon vacancies and dangling bonds in the rGO [54]. Figure 3d shows high-resolution of O1s XPS spectra of Cu_2O and Cu_2O-rGO-*x*. The features at 531.0 and 531.8 eV can be attributed to oxygen vacancy and adsorbed oxygen, respectively [44]. It can be seen that the intensities of two components are increased upon the increased decoration of rGO. As reported earlier [55], the binding of oxygen vacancies in the nanocrystalline Cu_2O with bicarbonate ions may be enhanced, which could promote the photoreduction of CO_2 discussed below.

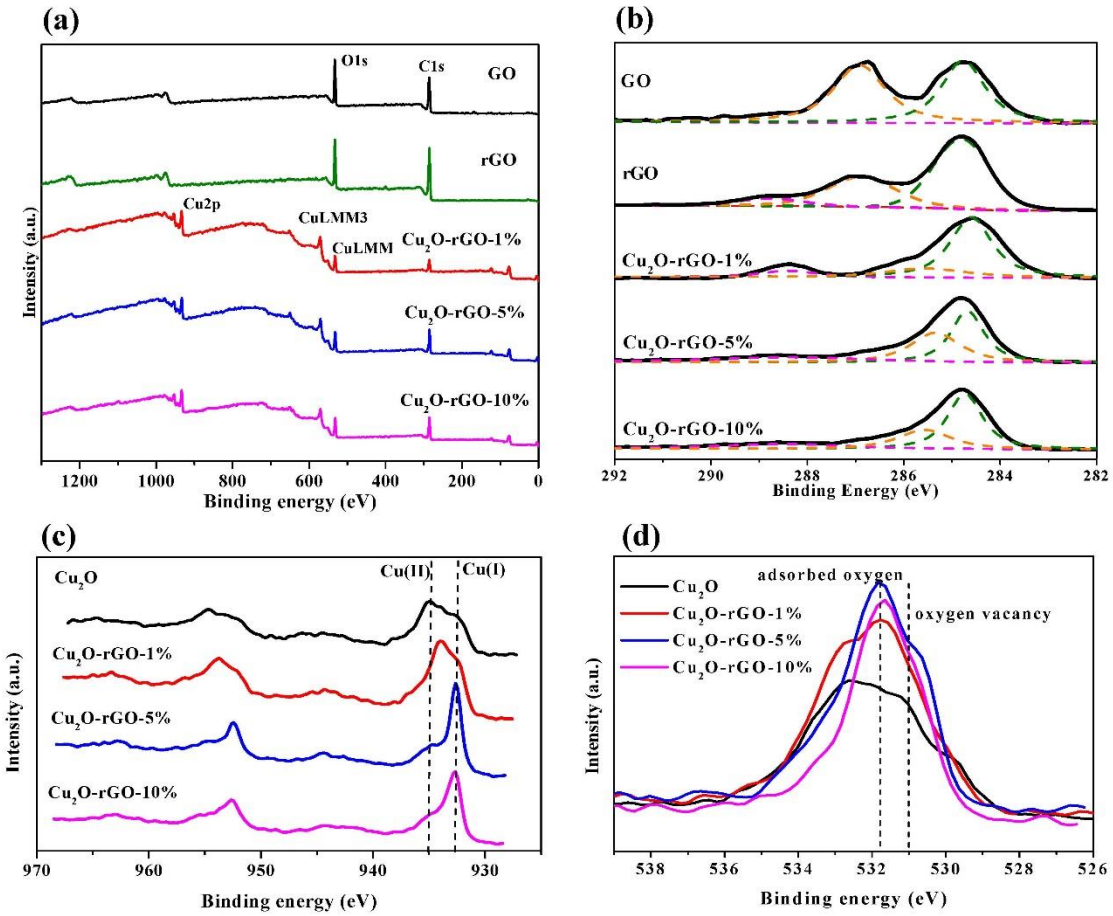

Figure 3. XPS spectra of various photocatalysts: (**a**) survey, (**b**) C 1s (**c**) Cu 2p and (**d**) O 1s regions.

The optical absorption of Cu_2O and Cu_2O-rGO-*x* composites was investigated by diffuse reflectance ultraviolet/visible (UV/Vis) spectra. The UV/Vis spectra of Cu_2O and Cu_2O-rGO-*x* show a wide absorption profile from 300 to 600 nm, as displayed in Figure 4a. In addition, the absorption intensities of Cu_2O-rGO-*x* composites are relatively enhanced in the absorption wavelength >600 nm regions if compared with those of Cu_2O. The increased absorption intensity of Cu_2O-rGO-*x* composites depends on the amounts of rGO in the composites; i.e., the intensity is increased with increasing amounts of rGO. Therefore, the rGO could cause a red shift to promote the absorption ability in the visible region of Cu_2O. Figure 4b shows that the band gap of Cu_2O is reduced as Cu_2O combined with rGO. Their corresponding threshold wavelength can be obtained and is shown in Table 1. The band gap of the pure Cu_2O nanocrystal is assessed to be 2.18 and those of Cu_2O-rGO-*x* composites are decreased to be 2.16–2.06 with increasing contents of rGO in the Cu_2O-rGO-*x* composites. A red-shift

absorbance and the narrower bad gap of composites means that it can easily absorb the visible light. Therefore, the incorporation of rGO onto the Cu_2O is good for the absorption of visible light during photocatalytic reduction.

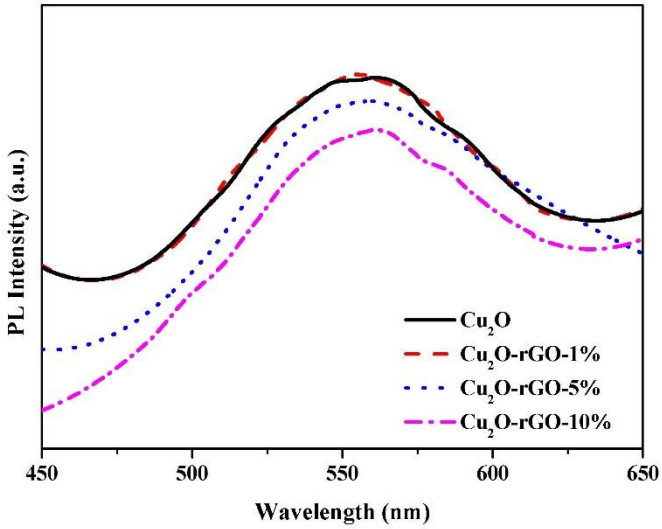

Figure 4. The photo-luminescence (PL) pattern of Cu_2O and Cu_2O-rGO-*x* (*x* = 1%, 5% and 10%).

Table 1. Energy gaps and threshold wavelength of Cu_2O and Cu_2O-rGO-*x* (*x* = 1%, 5% and 10%).

Sample	Energy Gap (eV)	Threshold Wavelength (nm)
Cu_2O	2.18	570.11
Cu_2O-rGO-1%	2.16	573.01
Cu_2O-rGO-5%	2.16	574.87
Cu_2O-rGO-10%	2.06	603.11

The rates of the electron–hole recombination can be determined by photo-luminescence (PL) with the exited wavelength at 325 nm. The peak position is related to the band gap value of photocatalysts and the intensity of the peak represents the rates of the electron–hole recombination. A higher intensity of peaks indicates a greater rate of electron–hole recombination. On the other hand, a lower intensity of peaks means an inferior rate of electron–hole recombination. As can be seen in Figure 5, the Cu_2O-rGO-10% composites have the lowest intensity of PL peaks, which suggests that they have the lowest recombination rates. Accordingly, the rate of electron–hole recombination can be reduced by decorating rGO on Cu_2O, and the photo-exited electrons can be effectively transferred from Cu_2O to rGO to separate electrons and holes [56–59].

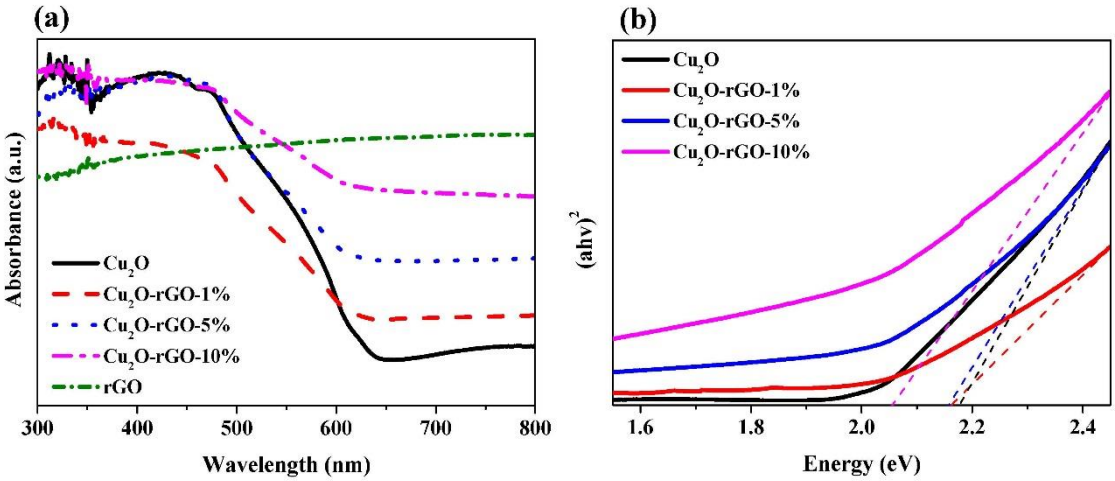

Figure 5. (**a**) UV-VIS spectra and (**b**) their corresponding Kubelka–Munk plots of Cu_2O and various Cu_2O-rGO-x (x = 1%, 5% and 10%) photocatalysts.

The photoconversion of CO_2 into methanol photocatalyzed by Cu_2O and Cu_2O-rGO-x composites was examined under visible light for 20 h. In this study, the possible products, such as HCHO and HCOOH, which were confirmed by injecting the standard solution of respective compounds, were not detected. Only methanol was observed as the main product. In order to check the formation of methanol during photocatalytic reaction, we performed three blank experiments. It can be seen that no methanol can be obtained without the assistance of photocatalysts, light irradiation and the existence of CO_2 (see Table 2). Moreover, Figure 6 shows that the contents of rGO have a great effect on the photocatalytic activity of Cu_2O nanocrystals. The methanol yields varied with the contents of rGO follow the order Cu_2O-rGO-5% > Cu_2O-rGO-1% > Cu_2O-rGO-10% > Cu_2O. The yields of methanol are 9.76, 47.91, 335.26 and 12.41 μmol g^{-1}cat, corresponding to Cu_2O, Cu_2O-rGO-1%, Cu_2O-rGO-5% and Cu_2O-rGO-10%, respectively after 20 h of visible-light irradiation. Among these prepared photocatalysts, the Cu_2O-rGO-5% composites possess the best activity for the photoreduction of CO_2. It is concluded that the suitable amounts of rGO which are incorporated onto Cu_2O would have a positive impact on the photocatalytic performance of CO_2 reduction. According to the UV-Vis spectrum, the adsorption intensity of Cu_2O in the visible regions is promoted and the energy gap of Cu_2O is reduced by combining with rGO, indicating that Cu_2O-rGO-x can easily absorb visible light to generate electron–hole pairs which can be utilized to reduce CO_2. The PL patterns indicate that the peak intensities are declined with increasing ratios of rGO to Cu_2O, suggesting that the rGO can effectively prevent the electron–hole pairs from recombination. The SEM/TEM images show that the aggregation of Cu_2O nanocrystals can be suppressed by decorating with rGO, and thus the activity sites are also increased. XPS spectra show that rGO nanosheets served as the protective layers to prevent the photoreduction and oxidation of Cu_2O by photogenerated electrons and water, respectively, which enhance the stability of Cu_2O during the photocatalytic reaction. Consequently, the methanol yield of Cu_2O-rGO-5% composites (355.26 μmol g^{-1}cat) is ca. 36 times higher than that of pure Cu_2O nanocrystal (9.76 μmol g^{-1}cat). Additionally, the apparent quantum efficiency (AQE) of Cu_2O-rGO-5% under visible-light illumination was estimated to be 0.724%. However, the photocatalytic activity is observed to be decreased when the ratio (rGO/Cu_2O) is further increased to 10%. This result may be due to the fact that excessive rGO would deteriorate the crystal facet of Cu_2O as well as obstructing light from reaching the surface of Cu_2O nanocrystals which generated fewer electron–hole pairs, thereby decreasing the reduction of CO_2 [52].

Table 2. Conditions for the photocatalytic reduction of CO_2.

Sample	Reaction Precursor	Visible Light Illumination (λ > 400 nm)	Methanol Yield (μmol g^{-1}-cat)
None	CO_2	O	None
Cu_2O	CO_2	O	9.76
Cu_2O-rGO-1%	CO_2	O	47.91
Cu_2O-rGO-5%	CO_2	O	355.26
Cu_2O-rGO-5%	CO_2	X	None
Cu_2O-rGO-5%	N_2	O	None
Cu_2O-rGO-10%	CO_2	O	12.41

All experiments were carried out at 27 °C with 0.5 mg-cat/mL-solvent.

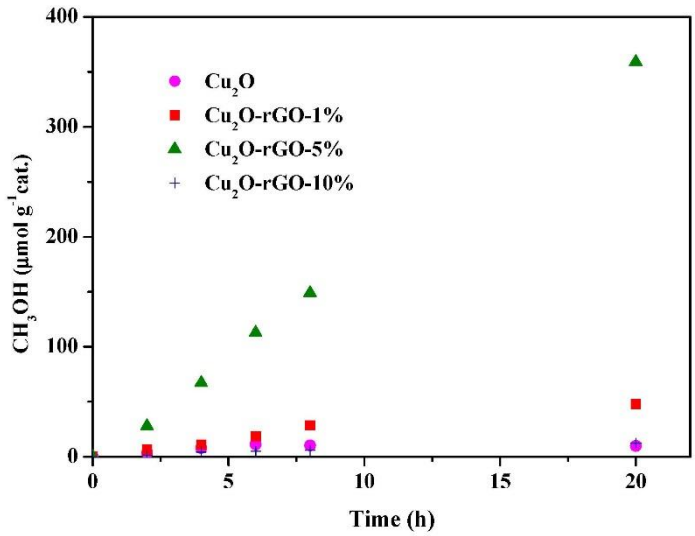

Figure 6. Photocatalytic methanol formation by Cu_2O and Cu_2O-rGO-*x* (*x* = 1%, 5% and 10%) under visible light irradiation.

Combining the results mentioned above, a possible mechanism of photocatalytic CO_2 reduction by Cu_2O-rGO-*x* composites is illustrated in Figure 7. The Cu_2O-rGO-*x* composites possess band gaps of ca. 2.1 eV with more negative reduction potential than that of methanol formation (E = −0.38 V vs. NHE at pH = 7) and slightly more positive oxidation potential than that of oxygen evolution (E = 0.81 V vs. NHE at pH = 7) [24]. The photogenerated electrons are transferred to highly conductive rGO to react with CO_2 or O_2 which have two lone pairs of electrons for the formation of π-electrons bindings on the rGO surface. As such, the recombination of electron–hole pairs would be hindered significantly, which is important for the electron-dominated reduction reaction [50]. More importantly, the removal of electrons from the conduction bands of Cu_2O via rGO can prevent the photoreduction of Cu_2O and thus enhance the photostability [60]. In addition, the protection of rGO from the oxidation of Cu_2O by water may maintain the copper in the Cu(I) state [61]. In Figure S1, the XRD pattern confirms that the crystal phase of Cu_2O is intact after 20 h of photocatalytic reaction. It is noteworthy that the dominant product of methanol may be caused by the exposed (110) facets of Cu_2O on which hydrogen may perform the addition to the oxygen atom in the bicarbonate rather than a carbon atom. This finding is similar to the pervious study [62]. In terms of photogenerated holes, the evolution of oxygen gas (ca. 4.9 μmol g^{-1}cat after 20 h of visible-light irradiation) implies that the occurrence of water splitting would serve as the hole scavenger, which hinders the recombination of electron–hole pairs. However, the lower amounts of evoluted oxygen after 20 h of photocatalytic reaction may be ascribed to the possibility of carbon corrosion and oxygen reduction.

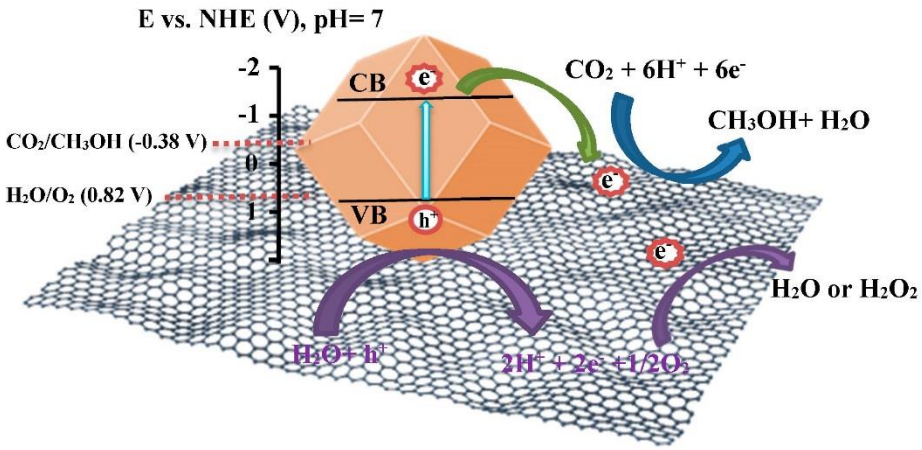

Figure 7. A possible mechanism of CO_2 photoreduction catalyzed by Cu_2O-rGO-*x* under visible light irradiation.

4. Conclusions

In summary, crystal Cu_2O photocatalysts incorporated with various amounts of rGO (1–10%) are prepared via a simple solution-chemistry route. Among the prepared Cu_2O-rGO-*x* composites, we found that the Cu_2O-rGO-5% (5 wt.% of rGO) photocatalysts possess the superior photocatalytic performance toward CO_2 reduction; i.e., after visible light illumination for 20 h, the methanol yield of Cu_2O-rGO-5% composites can reach 355.26 μmol g^{-1}cat, which is about 36 times that of pure Cu_2O photocatalysts. This remarkable enhancement in the CO_2 photoreduction activity may be due to the increased intensity of visible-light absorption in the Cu_2O (identified by UV-VIS), reduced recombination of electron–hole pairs (proven by PL), enhanced dispersion of crystal Cu_2O (examined by SEM/TEM) and stabilization of Cu_2O (evidenced by XPS). Accordingly, the visible-light-driven photocatalytic reduction of CO_2 by Cu_2O-rGO-*x* composites could provide a possible opportunity for CO_2 conversion by using sunlight energy.

Supplementary Materials: The following are available online at http://www.mdpi.com/2071-1050/10/11/4145/s1, Figure S1: XRD patterns of the fresh and used photocatalysts after 20 h of photocatalytic reaction.

Author Contributions: Designing, writing, review & editing the paper, S.-H.L.; doing the experiments and analyzing the data, J.-S.L. All authors reviewed and approved the manuscript.

Acknowledgments: We are gratefully appreciated the support of this study by the Ministry of Science and Technology of Taiwan (grant number: MOST 105-2221-E-006-015-MY5).

Conflicts of Interest: The authors declare no conflict of interest.

References

1. DeCicco, J.M. Methodological issues regarding biofuels and carbon uptake. *Sustainability* **2018**, *10*, 1581. [CrossRef]
2. Sethupathi, S.; Zhang, M.; Rajapaksha, A.U.; Lee, S.R.; Nor, N.M.; Mohamed, A.R.; Al-Wabel, M.; Lee, S.S.; Ok, Y.S. Biochars as potential adsorbers of CH_4, CO_2 and H_2S. *Sustainability* **2017**, *9*, 121. [CrossRef]
3. Wieckol-Ryk, A.; Krzemien, A.; Smolinski, A.; Lasheras, F.S. Analysis of biomass blend co-firing for post combustion CO_2 capture. *Sustainability* **2018**, *10*, 923. [CrossRef]
4. Yang, M.-Q.; Xu, Y.-J. Photocatalytic conversion of CO_2 over graphene-based composites: Current status and future perspective. *Nanoscale Horiz.* **2016**, *1*, 185–200. [CrossRef]
5. Li, X.; Yu, J.; Jaroniec, M. Hierarchical photocatalysts. *Chem. Soc. Rev.* **2016**, *45*, 2603–2636. [CrossRef] [PubMed]
6. Liu, J.H.; Sun, Y.W.; Jiang, X.; Zhang, A.F.; Song, C.S.; Guo, X.W. Pyrolyzing ZIF-8 to N-doped porous carbon facilitated by iron and potassium for CO_2 hydrogenation to value-added hydrocarbons. *J. CO_2 Util.* **2018**, *25*, 120–127. [CrossRef]

7. Zhao, G.; Huang, X.; Wang, X.; Wang, X. Progress in catalyst exploration for heterogeneous CO_2 reduction and utilization: A critical review. *J. Mater. Chem. A* **2017**, *5*, 21625–21649. [CrossRef]
8. Ola, O.; Maroto-Valer, M.M. Review of material design and reactor engineering on TiO_2 photocatalysis for CO_2 reduction. *J. Photochem. Photobiol. C* **2015**, *24*, 16–42. [CrossRef]
9. Li, K.; Peng, B.; Peng, T. Recent advances in heterogeneous photocatalytic CO_2 conversion to solar fuels. *ACS Catal.* **2016**, *6*, 7485–7527. [CrossRef]
10. Rao, H.; Schmidt, L.C.; Bonin, J.; Robert, M. Visible-light-driven methane formation from CO_2 with a molecular iron catalyst. *Nature* **2017**, *548*, 74–77. [CrossRef] [PubMed]
11. Perini, J.A.L.; Cardoso, J.C.; de Brito, J.F.; Zanoni, M.V.B. Contribution of thin films of ZrO_2 on TiO_2 nanotubes electrodes applied in the photoelectrocatalytic CO_2 conversion. *J. CO_2 Util.* **2018**, *25*, 254–263. [CrossRef]
12. De Brito, J.F.; Hudari, F.F.; Zanoni, M.V.B. Photoelectrocatalytic performance of nanostructured p-n junction $NtTiO_2$/NsCuO electrode in the selective conversion of CO_2 to methanol at low bias potentials. *J. CO_2 Util.* **2018**, *24*, 81–88. [CrossRef]
13. Li, Q.; Li, X.; Wageh, S.; Al-Ghamdi, A.A.; Yu, J. CdS/Graphene nanocomposite photocatalysts. *Adv. Energy Mater.* **2015**, *5*, 1500010. [CrossRef]
14. Hou, J.; Cheng, H.; Takeda, O.; Zhu, H. Three-dimensional bimetal-graphene-semiconductor coaxial nanowire arrays to harness charge flow for the photochemical reduction of carbon dioxide. *Angew. Chem. Int. Ed.* **2015**, *54*, 8480–8484. [CrossRef] [PubMed]
15. Penconi, M.; Rossi, F.; Ortica, F.; Elisei, F.; Gentili, P.L. Heterojunction p-n-p Cu_2O/S-TiO_2/CuO: Synthesis and application to photocatalytic conversion of CO_2 to methane. *J. CO_2 Util.* **2017**, *20*, 91–96.
16. Pan, H.Q.; Steiniger, A.; Heagy, M.D.; Chowdhury, S. Efficient production of formic acid by simultaneous photoreduction of bicarbonate and oxidation of glycerol on gold-TiO_2 composite under solar light. *J. CO_2 Util.* **2017**, *22*, 117–123. [CrossRef]
17. Zhang, D.; Maimaiti, H.; Awati, A.; Yisilamu, G.; Sun, F.; Wei, M. Synthesis and photocatalytic CO_2 reduction performance of Cu_2O/coal-based carbon nanoparticle composites. *Chem. Phys. Lett.* **2018**, *700*, 27–35.
18. Abdullah, H.; Khan, M.M.R.; Ong, H.R.; Yaakob, Z. Modified TiO_2 photocatalyst for CO_2 photocatalytic reduction: An overview. *J. CO_2 Util.* **2017**, *22*, 15–32. [CrossRef]
19. Zubair, M.; Razzaq, A.; Grimes, C.A.; In, S.I. Cu_2ZnSnS_4 (CZTS)-ZnO: A noble metal-free hybrid Z-scheme photocatalyst for enhanced solar-spectrum photocatalytic conversion of CO_2 to CH_4. *J. CO_2 Util.* **2017**, *20*, 301–311. [CrossRef]
20. Tan, L.-L.; Ong, W.-J.; Chai, S.-P.; Mohamed, A.R. Visible-light-activated oxygen-rich TiO_2 as next generation photocatalyst: Importance of annealing temperature on the photoactivity toward reduction of carbon dioxide. *Chem. Eng. J.* **2016**, *283*, 1254–1263. [CrossRef]
21. Akple, M.S.; Low, J.; Liu, S.W.; Cheng, B.; Yu, J.G.; Ho, W.K. Fabrication and enhanced CO_2 reduction performance of N-self-doped TiO_2 microsheet photocatalyst by bi-cocatalyst modification. *J. CO_2 Util.* **2016**, *16*, 442–449. [CrossRef]
22. Liu, S.-H.; Syu, H.-R. One-step fabrication of N-doped mesoporous TiO_2 nanoparticles by self-assembly for photocatalytic water splitting under visible light. *Appl. Energy* **2012**, *100*, 148–154. [CrossRef]
23. Liu, S.-H.; Syu, H.-R. High visible-light photocatalytic hydrogen evolution of C,N-codoped mesoporous TiO_2 nanoparticles prepared via an ionic-liquid-template approach. *Int. J. Hydrogen Energy* **2013**, *38*, 13856–13865. [CrossRef]
24. Yu, L.; Li, G.; Zhang, X.; Ba, X.; Shi, G.; Li, Y.; Wong, P.K.; Yu, J.C.; Yu, Y. Enhanced activity and stability of carbon-decorated cuprous oxide mesoporous nanorods for CO_2 reduction in artificial photosynthesis. *ACS Catal.* **2016**, *6*, 6444–6454. [CrossRef]
25. Siegfried, M.J.; Choi, K.S. Elucidating the effect of additives on the growth and stability of Cu_2O surfaces via shape transformation of pre-grown crystals. *J. Am. Chem. Soc.* **2006**, *128*, 10356–10357. [CrossRef] [PubMed]
26. An, X.Q.; Li, T.; Wen, B.; Tang, J.W.; Hu, Z.Y.; Liu, L.M.; Qu, J.H.; Huang, C.P.; Liu, H.J. New Insights into defect-Mediated heterostructures for photoelectrochemical water splitting. *Adv. Energy Mater.* **2016**, *6*, 1502268. [CrossRef]
27. Wu, J.; Xu, K.; Liu, Q.Z.; Ji, Z.; Qu, C.H.; Zhang, H.; Guan, Y.; He, P.; Zhu, L.J. Controlling dominantly reactive (010) facets and impurity level by in-situ reduction of $BiOIO_3$ for enhancing photocatalytic activity. *Appl. Catal. B Environ.* **2018**, *232*, 135–145. [CrossRef]

28. He, W.J.; Sun, Y.J.; Jiang, G.M.; Huang, H.W.; Zhang, X.M.; Dong, F. Activation of amorphous Bi_2WO_6 with synchronous Bi metal and Bi_2O_3 coupling: Photocatalysis mechanism and reaction pathway. *Appl. Catal. B Environ.* **2018**, *232*, 340–347. [CrossRef]
29. Tan, C.F.; Zing, A.; Chen, Z.H.; Liow, C.H.; Phan, H.T.; Tan, H.R.; Xu, Q.H.; Ho, G.W. Inverse stellation of CuAu-ZnO multimetallic-semiconductor nanostartube for plasmon-enhanced photocatalysis. *ACS Nano* **2018**, *12*, 4512–4520. [CrossRef] [PubMed]
30. Cao, C.S.; Wen, Z.H. Cu nanoparticles decorating rGO nanohybrids as electrocatalyst toward CO_2 reduction. *J. CO_2 Util.* **2017**, *22*, 231–237. [CrossRef]
31. Ma, Y.J.; Zhu, X.Z.; Xu, S.S.; He, G.L.; Yao, L.; Hu, N.T.; Su, Y.J.; Feng, J.; Zhang, Y.F.; Yang, Z. Gold nanobipyramid@cuprous oxide jujube-like nanostructures for plasmon-enhanced photocatalytic performance. *Appl. Catal. B Environ.* **2018**, *234*, 26–36. [CrossRef]
32. Kerour, A.; Boudjadar, S.; Bourzami, R.; Allouche, B. Eco-friendly synthesis of cuprous oxide (Cu_2O) nanoparticles and improvement of their solar photocatalytic activities. *J. Solid State Chem.* **2018**, *263*, 79–83. [CrossRef]
33. Kumar, S.; Parlett, C.M.A.; Isaacs, M.A.; Jowett, D.V.; Douthwaite, R.E.; Cockett, M.C.R.; Lee, A.F. Facile synthesis of hierarchical Cu_2O nanocubes as visible light photocatalysts. *Appl. Catal. B Environ.* **2016**, *189*, 226–232. [CrossRef]
34. Shang, Y.; Guo, L. Facet-controlled synthetic strategy of Cu_2O-based crystals for catalysis and sensing. *Adv. Sci.* **2015**, *2*, 1500140. [CrossRef] [PubMed]
35. Zhang, W.; Ma, Y.J.; Yang, Z.; Tang, X.H.; Li, X.L.; He, G.L.; Cheng, Y.Q.; Fang, Z.B.; He, R.; Zhang, Y.F. Analysis of synergistic effect between graphene and octahedral cuprous oxide in cuprous oxide-graphene composites and their photocatalytic application. *J. Alloys Compd.* **2017**, *712*, 704–713. [CrossRef]
36. Liu, S.-H.; Lu, J.-S. Facet-dependent cuprous oxide nanocrystals decorated with graphene as durable photocatalysts under visible light. *Nanomaterials* **2018**, *8*, 423. [CrossRef] [PubMed]
37. Liu, S.-H.; Lu, J.-S.; Yang, S.-W. Highly visible-light-responsive Cu_2O/rGO decorated with Fe_3O_4@SiO_2 nanoparticles as a magnetically recyclable photocatalyst. *Nanotechnology* **2018**, *29*, 305606. [CrossRef] [PubMed]
38. Handoko, A.D.; Tang, J. Controllable proton and CO_2 photoreduction over Cu_2O with various morphologies. *Int. J. Hydrog. Energy* **2013**, *38*, 13017–13022. [CrossRef]
39. Ba, X.; Yan, L.L.; Huang, S.; Yu, J.G.; Xia, X.J.; Yu, Y. New way for CO_2 reduction under visible light by a combination of a Cu electrode and semiconductor thin film: Cu_2O conduction type and morphology effect. *J. Phys. Chem. C* **2014**, *118*, 24467–24478. [CrossRef]
40. Gusain, R.; Kumar, P.; Sharma, O.P.; Jain, S.L.; Khatri, O.P. Reduced graphene oxide–CuO nanocomposites for photocatalytic conversion of CO_2 into methanol under visible light irradiation. *Appl. Catal. B Environ.* **2016**, *181*, 352–362. [CrossRef]
41. Schreier, M.; Gao, P.; Mayer, M.T.; Luo, J.; Moehl, T.; Nazeeruddin, M.K.; Tilley, S.D.; Grätzel, M. Efficient and selective carbon dioxide reduction on low cost protected Cu_2O photocathodes using a molecular catalyst. *Energy Environ. Sci.* **2015**, *8*, 855–861. [CrossRef]
42. Lee, C.; Shin, K.; Lee, Y.J.; Jung, C.; Lee, H.M. Effects of shell thickness on Ag-Cu_2O core-shell nanoparticles with bumpy structures for enhancing photocatalytic activity and stability. *Catal. Today* **2018**, *303*, 313–319. [CrossRef]
43. Niu, W.Z.; Moehl, T.; Cui, W.; Wick-Joliat, R.; Zhu, L.P.; Tilley, S.D. Extended light harvesting with dual Cu_2O-based photocathodes for high efficiency water splitting. *Adv. Energy Mater.* **2018**, *8*, 1702323. [CrossRef]
44. Periasamy, A.P.; Ravindranath, R.; Kumar, S.M.S.; Wu, W.P.; Jian, T.R.; Chang, H.T. Facet- and structure-dependent catalytic activity of cuprous oxide/polypyrrole particles towards the efficient reduction of carbon dioxide to methanol. *Nanoscale* **2018**, *10*, 11869–11880. [CrossRef] [PubMed]
45. Zhang, Q.; Huang, L.; Kang, S.; Yin, C.; Ma, Z.; Cui, L.; Wang, Y. CuO/Cu_2O nanowire arrays grafted by reduced graphene oxide: Synthesis, characterization, and application in photocatalytic reduction of CO_2. *RSC Adv.* **2017**, *7*, 43642–43647. [CrossRef]
46. Liu, S.-H.; Wei, Y.-S.; Lu, J.-S. Visible-light-driven photodegradation of sulfamethoxazole and methylene blue by Cu_2O/rGO photocatalysts. *Chemosphere* **2016**, *154*, 118–123. [CrossRef] [PubMed]
47. Xiang, Q.; Cheng, B.; Yu, J. Graphene-based photocatalysts for solar-fuel generation. *Angew. Chem. Int. Ed.* **2015**, *54*, 11350–11366. [CrossRef] [PubMed]

48. Dos Santos, T.C.; Ronconi, C.M. Self-assembled 3D mesoporous graphene oxides (MEGOs) as adsorbents and recyclable solids for CO_2 and CH_4 capture. *J. CO_2 Util.* **2017**, *20*, 292–300. [CrossRef]
49. Deerattrakul, V.; Dittanet, P.; Sawangphruk, M.; Kongkachuichay, P. CO_2 hydrogenation to methanol using Cu-Zn catalyst supported on reduced graphene oxide nanosheets. *J. CO_2 Util.* **2017**, *16*, 104–113. [CrossRef]
50. An, X.; Li, K.; Tang, J. Cu_2O/reduced graphene oxide composites for the photocatalytic conversion of CO_2. *ChemSusChem* **2014**, *7*, 1086–1093. [CrossRef] [PubMed]
51. Wang, A.; Li, X.; Zhao, Y.; Wu, W.; Chen, J.; Meng, H. Preparation and characterizations of Cu_2O/reduced graphene oxide nanocomposites with high photo-catalytic performances. *Powder Technol.* **2014**, *261*, 42–48. [CrossRef]
52. Liu, S.-H.; Yang, S.-W. Highly efficient cuprous oxide nanocrystals assisted with graphene for decolorization using visible light. *Water Air Soil Pollut.* **2018**, *229*, 67. [CrossRef]
53. Huang, W.C.; Lyu, L.M.; Yang, Y.C.; Huang, M.H. Synthesis of Cu_2O nanocrystals from cubic to rhombic dodecahedral structures and their comparative photocatalytic activity. *J. Am. Chem. Soc.* **2012**, *134*, 1261–1267. [CrossRef] [PubMed]
54. Guo, X.; Hao, C.; Jin, G.; Zhu, H.Y.; Guo, X.Y. Copper nanoparticles on graphene support: An efficient photocatalyst for coupling of nitroaromatics in visible light. *Angew. Chem. Int. Ed.* **2014**, *53*, 1973–1977. [CrossRef] [PubMed]
55. Tu, K.; Wang, Q.; Lu, A.; Zhang, L. Portable visible-light photocatalysts constructed from Cu_2O nanoparticles and graphene oxide in cellulose matrix. *J. Phys. Chem. C* **2014**, *118*, 7202–7210. [CrossRef]
56. Zou, W.; Zhang, L.; Liu, L.; Wang, X.; Sun, J.; Wu, S.; Deng, Y.; Tang, C.; Gao, F.; Dong, L. Engineering the Cu_2O–reduced graphene oxide interface to enhance photocatalytic degradation of organic pollutants under visible light. *Appl. Catal. B Environ.* **2016**, *181*, 495–503. [CrossRef]
57. Zhang, W.; Li, X.; Yang, Z.; Tang, X.; Ma, Y.; Li, M.; Hu, N.; Wei, H.; Zhang, Y. In situ preparation of cubic Cu_2O-RGO nanocomposites for enhanced visible-light degradation of methyl orange. *Nanotechnology* **2016**, *27*, 265703. [CrossRef] [PubMed]
58. Cai, J.; Liu, W.; Li, Z. One-pot self-assembly of Cu_2O/RGO composite aerogel for aqueous photocatalysis. *Appl. Surf. Sci.* **2015**, *358*, 146–151. [CrossRef]
59. Zhang, L.X.; Li, N.; Jiu, H.F.; Qi, G.S.; Huang, Y.J. ZnO-reduced graphene oxide nanocomposites as efficient photocatalysts for photocatalytic reduction of CO_2. *Ceram. Int.* **2015**, *41*, 6256–6262. [CrossRef]
60. Ma, G.X.; Jia, R.R.; Zhao, J.H.; Wang, Z.J.; Song, C.; Jia, S.P.; Zhu, Z.P. Nitrogen-doped hollow carbon nanoparticles with excellent oxygen reduction performances and their electrocatalytic kinetics. *J. Phys. Chem. C* **2011**, *115*, 25148–25154. [CrossRef]
61. Xiang, C.X.; Kimball, G.M.; Grimm, R.L.; Brunschwig, B.S.; Atwater, H.A.; Lewis, N.S. 820 mV open-circuit voltages from Cu_2O/CH_3CN junctions. *Energy Environ. Sci.* **2011**, *4*, 1311–1318. [CrossRef]
62. Yuan, J.L.; Wang, X.; Gu, C.H.; Sun, J.J.; Ding, W.M.; Wei, J.J.; Zuo, X.Y.; Hao, C.J. Photoelectrocatalytic reduction of carbon dioxide to methanol at cuprous oxide foam cathode. *RSC Adv.* **2017**, *7*, 24933–24939. [CrossRef]